Origin of negative magnetoresistance of GaAs/(Ga,Mn)As core-shell nanowires

Christian Butschkow,[1] Elisabeth Reiger,[1] Andreas Rudolph,[1] Stefan Geißler,[1] Daniel Neumaier,[1] Marcello Soda,[1] Dieter Schuh,[1] Georg Woltersdorf,[1] Werner Wegscheider,[2] and Dieter Weiss[1]

[1]*Institute of Experimental and Applied Physics, University of Regensburg, 93053 Regensburg, Germany*

[2]*ETH Zürich, 8093 Zürich, Switzerland*

(Received 11 January 2013; published 6 June 2013)

We explore the anisotropy of the magnetoresistance of individual GaAs/(Ga,Mn)As core-shell nanowires which feature a strong negative magnetoresistance (NMR) and a very large magnetic anisotropy field. Our analysis of the magnetoresistance shows that the resistance anisotropy is dominated by the effective magnetic field and that the origin of the NMR is related to spin scattering rather than to weak localization in (Ga,Mn)As core-shell nanowires.

DOI: 10.1103/PhysRevB.87.245303 PACS number(s): 75.47.−m, 72.10.Di, 75.50.Pp, 81.07.Gf

Since the discovery of (Ga,Mn)As in 1996,[1] the electrical transport properties, Curie temperature, and magnetic anisotropies of this dilute magnetic semiconductor (DMS) material have been widely explored both experimentally and theoretically [see, e.g., Ref. 2 and references therein]. Early on, it was noticed that (Ga,Mn)As films exhibit a decreasing magnetoresistance with increasing magnetic field, denoted as negative magnetoresistance (NMR). This effect was first attributed to the suppression of spin fluctuations by the external magnetic field,[3] but later to orbital weak localization.[4] Weak localization can explain the fact that the NMR does not saturate even for high magnetic fields up to 30 T (Ref. 5), where all spins should be aligned with the external magnetic field. While the suppression of weak localization scales with the externally applied magnetic flux, spin disorder effects, namely spin fluctuations and spin waves, are sensitive to the internal effective magnetic field H_{eff}. The NMR effect is also found in lithographically defined nanowires with $\Delta R/R$ of the order of a few percent. The size of the NMR effect is significantly enhanced with $\Delta R/R$ of order several 10% with increasing disorder, introduced, e.g., by He ion irradiation.[6] Properties of epitaxially grown (Ga,Mn)As nanowires, in contrast, are much less explored as the low growth temperatures needed to avoid MnAs formation[1] prevent direct application of the vapor-liquid-solid (VLS) mechanism.[7] Attempts to implant Mn into GaAs nanowires by ion beam irradiation resulted in strongly disordered systems featuring hopping transport.[8] Here, we explore the magnetotransport properties of core-shell nanowires which exhibit, compared to lithographically defined wires, a topologically different geometry, i.e., a geometry without edges, in which a ferromagnetic (Ga,Mn)As shell, grown at low temperatures, is "wrapped" around a GaAs core. The nanowires show a uniaxial magnetic anisotropy along the wire axis[9] in contrast to a similar system in which (Ga,Mn)As was replaced by the metal MnAs (Refs. 10 and 11). The unique property set of our nanowires is a strong uniaxial anisotropy and a very pronounced NMR. With such samples it is possible to unveil the role of the effective magnetic field on electrical transport. We demonstrate that the NMR dominates both low field and high field magnetoresistance, i.e., also at small magnetic fields where in planar (Ga,Mn)As films the anisotropic magnetoresistance (AMR) effect prevails,[12] suggesting that spin scattering is the principal mechanism causing NMR in our samples.

The core-shell nanowires used here were grown by molecular beam epitaxy using gold as a catalyst.[7] The GaAs core nanowires have diameters ranging between 40 and 80 nm and lengths between 500 and 4.5 μm. The (Ga,Mn)As shell was deposited on the side facets of the core at low temperatures of 205 °C to prevent MnAs segregation. The shell has an average thickness of ∼20 nm and contains approximately 5% Mn. In bright field TEM images the GaAs core can be clearly distinguished from the shell [Fig. 1(b)]. The contrast stems from Mn interstitials in (Ga,Mn)As (Ref. 13) indicating that no pronounced Mn back-diffusion into the core takes place. This is also supported by energy dispersive x-ray spectroscopy (EDX) measurements (not shown). The absence of crystal

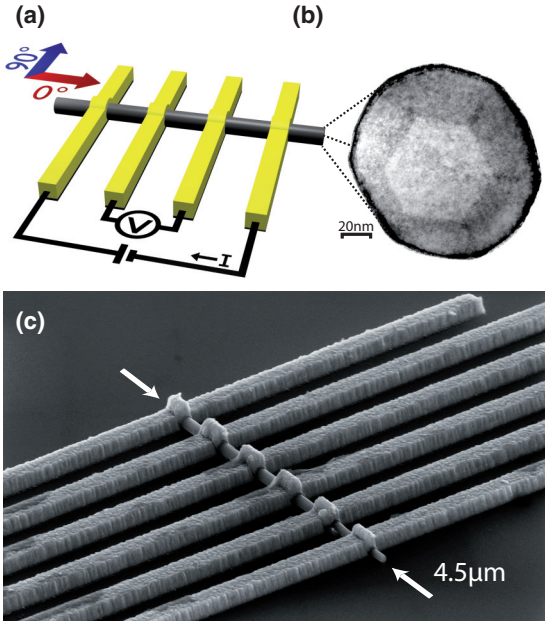

FIG. 1. (Color) (a) Schematic of the sample design and the experimental setup. The red and blue arrows define the plane in which the magnetic field is applied. (b) Bright-field transmission electron micrograph (TEM) of a core-shell nanowire cross section. The hexagonal core of GaAs with $\{11\bar{2}0\}$-oriented side facets is clearly distinguishable from the (Ga,Mn)As shell, which shows an epitaxial interface to the core. (c) Tilted scanning electron micrograph (SEM) of a contacted nanowire.

defects in high-resolution TEM (HRTEM) side-view images of the core-shell nanowires (not shown) demonstrates the epitaxial growth of (Ga,Mn)As on the core nanowires, i.e., the (Ga,Mn)As shell inherits the crystal structure of the core GaAs nanowire.

The crystal structure of the core-shell nanowires is determined by HRTEM and TEM diffractometry. The main central part of the nanowires, which is probed in our transport experiments, is predominantly of wurtzite crystal phase. At the tip and at the foot region of the nanowires small zincblende segments as well as stacking faults are more frequently observed. Such crystal phase mixing is typically observed in GaAs nanowires and is related to the catalytic growth mode.[14] In particular during the initial and final stages of the nanowire growth this crystal phase mixing is enhanced due to changes of the chemical composition of the AuGa catalyst droplet. Further details on the nanowire growth can be found in Ref. 9.

Previous superconducting interference device (SQUID) magnetometry on nanowire ensembles revealed a strong uniaxial magnetic anisotropy of the nanowires in the ferromagnetic state, with the magnetic easy axis pointing along the nanowire axis.[9] The anisotropy field H_A of the nanowire ensemble, defined as the magnetic field needed to align the magnetization completely in the direction of the magnetic hard axis, is $\sim$2 T at 4 K. The coercive field H_C, which denotes the switching of the magnetization when the external magnetic field is applied along the magnetic easy axis, is about 170 mT at 4 K. The Curie temperature T_C of all our wires is around 20 K. As SQUID measurements provide absolute values of the saturation magnetization M_S, we can calculate the uniaxial anisotropy constant K_U using $H_A = 2K_U/(\mu_0 M_S)$. This leads to a value of $K_U \approx 8500\ (\pm 1800)\ \mathrm{J/m^3}$ (Ref. 15).

The values for H_A and K_U are for core-shell nanowires significantly higher than for strained, lithographically defined (Ga,Mn)As nanostripes made from bulk (Ga,Mn)As films. Such planar nanostripes of width smaller than 500 nm also exhibit, due to strain relaxation,[16] a uniaxial anisotropy with the magnetic easy axis pointing along the stripe axis. Although these nanostripes have similar dimensions compared to the core-shell nanowires, they feature an anisotropy field which is by an order of magnitude smaller, ranging from $\mu_0 H_A \sim 180$ to 300 mT, and a uniaxial anisotropy constant that does not exceed $K_U \approx 1500\ \mathrm{J/m^3}$ (Refs. 16–18), a value which is about five times smaller when compared to the core-shell nanowires. Similar to the situation in etched narrow (Ga,Mn)As stripes, we assume that the strong uniaxial anisotropy is related to symmetry breaking due to an anisotropic relaxation of the crystal lattice. The radial geometry of the core-shell nanowires might permit very effective relaxation, and thus enhance the uniaxial anisotropy constant.

In contrast to SQUID characterization, where a large ensemble of nanowires—in our case $\sim 10^8$ NWs—is characterized simultaneously, in magnetotransport a single nanowire can be probed. For that we use the geometry displayed in Fig. 1. Individual nanowires were transferred to a SiO_2 substrate and contacted using electron beam lithography (EBL) [Fig. 1(c)]. Unless stated otherwise the transport measurements were performed in a four-terminal configuration [Fig. 1(a)], and carried out in a cryostat equipped with a superconducting coil enabling measurements at temperatures down to 1.4 K and in magnetic fields of up to 10 T. The nanowires exhibit a linear IV characteristic in the investigated temperature range. Therefore metallic transport behavior prevails and we do not expect any magnetoresistance effects related to tunneling or Coulomb blockade.[19,20] The samples were mounted on a rotatable sample holder, permitting to vary the angle between the applied magnetic field and the nanowire axis.

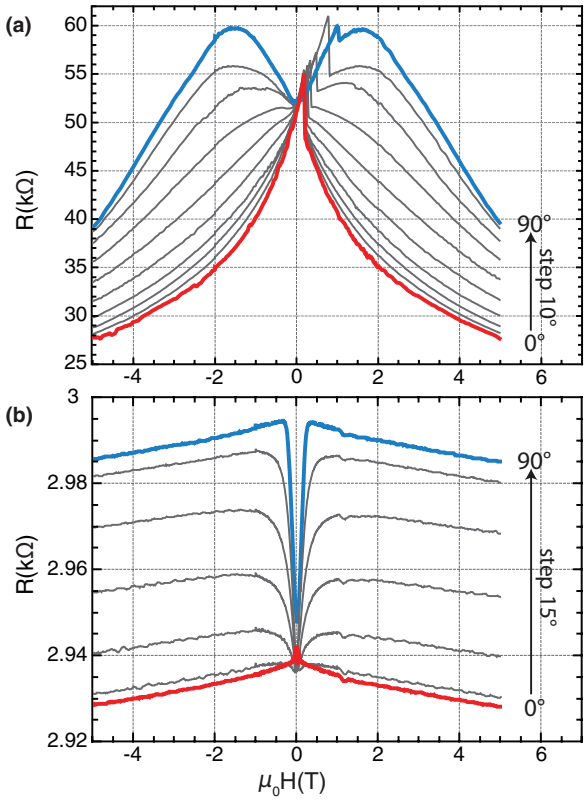

FIG. 2. (Color) Magnetoresistance curves at $T = 4$ K of (a) a single nanowire sample and (b) of a lithographically fabricated nanostripe array (Ref. 21) taken for different in-plane magnetic field directions between 0° (red) and 90° (blue). The field was swept from negative to positive values of H_0 (up sweep). The grey traces illustrate the gradual transition from the 0° to the 90° magnetoresistance trace. The small peak in (a) around $\sim$1 T in the topmost (blue) trace indicates that the field was not perfectly aligned along the 90° direction (accuracy of alignment: ±2°).

In total we investigated seven core-shell nanowires, which differ slightly in diameter (95–115 nm) and length (3.2–4.5 μm). All of these samples exhibited similar properties. We focus in the following on two nanowires. In Fig. 2 we compare the magnetoresistance traces of a core-shell nanowire [sample A, Fig. 2(a)] to the corresponding ones of a lithographically etched nanostripe array[21] [Fig. 2(b)]. For both sets of curves the magnetic field was applied in the sample plane (Fig. 1), varying the angle of the applied field with respect to the wire axis stepwise from 0° (magnetic field parallel to the wire axis) to 90° (magnetic field perpendicular to the wire axis).

The slight decrease of the resistance for fields larger than 0.25 T in Fig. 2(b) is the NMR of the planar nanowire array. The resistance change $\Delta R/R$ is of order 1%. The low field

magnetoresistance, featuring a positive magnetoresistance for the external magnetic field aligned perpendicular to the wire axis ($\varphi_H = 90^\circ$), is ascribed to the AMR effect. The AMR effect which typically exhibits a magnitude of 3% to 10% in (Ga,Mn)As (Ref. 22) leads to a change in resistance depending on the angle between the direction of the current flow (here along the nanowire axis) and the magnetization φ_M. In its simplest form AMR is described by $R(\varphi_M) = R_\perp - (R_\perp - R_\parallel)\cos^2(\varphi_M)$ for (Ga,Mn)As; i.e., it shows the largest resistance change for magnetic fields applied perpendicular to the current path.[22] Here, $R_\perp$ and $R_\parallel$ are $\sim$2.99 $k\Omega$ and $\sim$2.93 $k\Omega$. If the external field is oriented normal to the wire ($\varphi_H = 90^\circ$) the MR becomes maximum when the magnetization is also aligned normal to the wire axis ($\varphi_M = 90^\circ$). This occurs in Fig. 2(b) at $|\mu_0 H_0| \sim 250$ mT and constitutes the anisotropy field H_A of the planar nanowires. For a field sweep along the nanostripes [0° = magnetic easy axis, red curve in Fig. 2(b)], the resistance displays a small jump, hardly resolved on the field scale used here, at $\sim$50 mT when the magnetization switches by 180°. This resistance response to the switching of the magnetization cannot be explained by the AMR effect since a reversal by 180° would not cause a resistance change.

In contrast, the overall shape of the magnetoresistance of the core-shell nanowires differs significantly from the planar wire array. One obvious difference is a pronounced NMR effect of order $\Delta R/R \sim 50\%$, displayed in Fig. 2(a). Furthermore, for a magnetic field applied parallel to the wire axis [0°, red curve in Fig. 2(a)], a sharp resistance jump is found for the up sweep at $H_C \sim 220$ mT. This jump at the coercive field H_C is associated with the switching of magnetization by 180° along the magnetic easy direction, initiated by thermally activated domain wall nucleation and propagation. In contrast, magnetic field sweeps transverse to the nanowire axis [90°, blue curve in Fig. 2(a)] result in a steadily increasing magnetoresistance with positive slope in the low field region $|\mu_0 H_0| < 1.8$ T. This continuous positive MR reflects a coherent rotation of the magnetization, typical for magnetization reversal along a magnetic hard axis. When the magnitude of the external field equals the anisotropy field, the magnetization is aligned with the direction of the external field and the magnetoresistance exhibits a maximum. Upon further increase of the magnetic field strength, the magnetoresistance decreases. The grey curves in Fig. 2(a) illustrate the evolution of the MR from sweeps in parallel (0°) to perpendicular (90°) field configuration. The magnetization reversal is then a superposition of coherent rotation and domain wall propagation.

While the MR of the nanostripe array can be largely understood by a dominating AMR effect, superimposed by a small isotropic NMR effect, this is not the case for the magnetoresistance curves of the core-shell nanowire as (i) the magnitude of the observed effect is much too large, and (ii) the pronounced resistance jumps are not consistent with a dominating AMR effect. In the case of AMR a magnetization reversal by 180° would not lead to any magnetoresistance change. Below we show that our observations are in line with a picture in which the NMR is caused by spin-disorder scattering. Calculations by Kaul *et al.*[14] show, e.g., that the (effective) magnetic-field-induced suppression of magnon scattering can cause a sizable resistance decrease of several 10%. We therefore first summarize briefly the concept of the effective magnetic field in ferromagnetic materials.

In general, the precession of the magnetization $\vec{M}$ can be described by the equation of motion $\partial\vec{M}/\partial t = -\gamma[\vec{M} \times \vec{H}_{\text{eff}}]$ with the gyromagnetic factor γ and the effective field $\vec{H}_{\text{eff}}$. Precession takes place around the direction of the effective field $\vec{H}_{\text{eff}}$, which is parallel to the static equilibrium magnetization.[23] It can be shown that for small displacements of the magnetization $\vec{H}_{\text{eff}}$ is defined by the Gauss curvature of the free energy with respect to the polar and azimuthal angles of the magnetization vector $\vec{M}$. For the simple case of only uniaxial anisotropy, with the anisotropy constant K_U, and the Zeeman energy, the free energy density can be written as

$$E(\theta_M,\varphi_M) = K_U \sin^2(\theta_M)\sin^2(\varphi_M) + \mu_0 M_S H_0 \sin(\theta_M)\cos(\varphi_M - \varphi_H), \quad (1)$$

where θ_M and φ_M specify the azimuthal and polar angles of the magnetization with respect to the magnetic easy axis, while φ_H is the direction of the external magnetic field and M_S the saturation magnetization. When the static magnetization lies in the plane of the substrate ($\theta_M = 90^\circ$) Eq. (1) leads to an expression for the effective field

$$H_{\text{eff}} = \frac{1}{\mu_0 M_S \sin(\theta_M)}\sqrt{E_{\theta_M\theta_M}E_{\varphi_M\varphi_M} - E^2_{\theta_M\varphi_M}} \overset{\theta_M=90^\circ}{\approx} H_0\cos(\varphi_M - \varphi_H) + \frac{2K_U}{\mu_0 M_S}\cos(2\varphi_M), \quad (2)$$

where $E_{\theta_M\theta_M}, E_{\varphi_M\varphi_M}$, and $E_{\theta_M\varphi_M}$ are the second derivatives of the free energy density. The effective field consists of two terms; the first term is related to the applied external magnetic field, and the second term to the anisotropy field $H_A = \frac{2K_U}{\mu_0 M_S}$.

Since spins precess around the effective magnetic field, rather than the external magnetic field, we now interpret our magnetoresistance data using the concept of the effective field H_{eff}. Figures 3(a) and 3(b) display a magnification of the low field magnetoresistance of nanowire B for a magnetic field sweep along and perpendicular to the wire, respectively. As regards sample A, also this sample shows pronounced jumps when the magnetic field is applied parallel to the wire axis. The magnetoresistance measured along the nanowire axis [red trace Fig. 3(a)] shows a nearly linear increase of $R(H_0)$ from -1 to 0 T, and continues to increase beyond $\mu_0 H_0 = 0$ T until a resistance jump at the coercive field H_C occurs. The values of $\mu_0 H_C$, obtained for different nanowires at 4 K, range between 140 and 220 mT, and are in good agreement with the SQUID data of nanowire ensembles. Based on the linear behavior of the magnetoresistance trace in Fig. 3(a), we assume that the NMR changes, at least to first order, linearly with the effective magnetic field (NMR $= \frac{R(0)-R(H_{\text{eff}})}{R(0)} \propto -|\vec{H}_{\text{eff}}|$). The dashed grey lines in Figs. 3(a) and 3(b) display the computed effective field as a function of H_0. The calculation is based on Eq. (2), taking the value for H_A from the position of the resistance maxima in Fig. 3(b). Furthermore we need φ_M for each calculated datapoint. This was accomplished by simply minimizing the free energy equation (2) as a function of φ_M ($\frac{\partial E}{\partial \varphi_M} = 0; \frac{\partial^2 E}{\partial^2 \varphi_M} > 0$) while taking into account the changing external magnetic field.

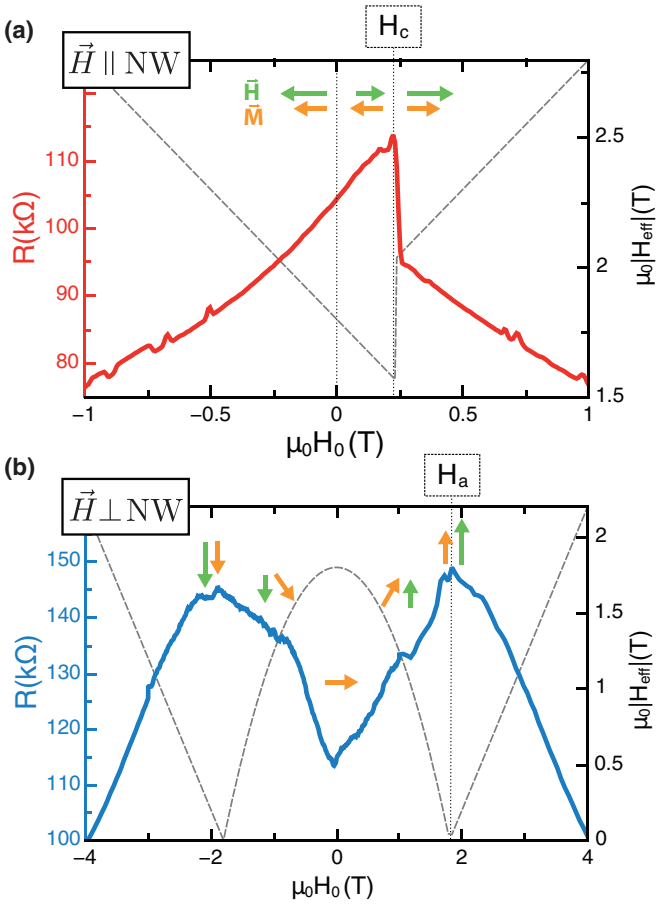

FIG. 3. (Color) Magnetotransport data at $T = 4$ K: (a) $\vec{H}$ parallel to the nanowire axis (0°). Arrows illustrate the relative orientation of external field and magnetization. The dashed grey line is the calculated effective magnetic field H_{eff}. The resistance jump reflects a change of the NMR as the effective magnetic field changes by $2H_C$ at this field. (b) $\vec{H}$ perpendicular to the nanowire axis (90°). Also here the MR follows inversely the calculated effective magnetic field (dashed line). The dashed lines in (a) and (b) show H_{eff} as a function of H_0 for the two magnetic field configurations with the corresponding y axis on the right side.

The calculated H_{eff} retraces closely but with inverted slope the magnetoresistance trace in Fig. 3(a). At -1 T the magnetization is aligned with the external magnetic field ($\varphi_M = 180°, \varphi_H = 180°$). Sweeping the field up, H_{eff} decreases linearly, paralleled by a linear increase of $R(H_0)$. This linear increase continues even beyond 0 T since the magnetization continues to stay in its initial direction. This results in an antiparallel alignment of magnetization and external field ($\varphi_M = 180°, \varphi_H = 0°$). This antiparallel configuration causes the effective magnetic field to decrease further until the magnetization is forced to switch its direction by 180°. Prior to the magnetization reversal, one has $H_{\text{eff},1} = -H_C + H_A$ since $H_0 = H_C$ [Eq. (2)]. Immediately after the jump, the magnetization aligns with the external field ($\varphi_M = 0°, \varphi_H = 0°$) and one obtains $H_{\text{eff},2} = H_C + H_A$. Thus, the resistance jump reflects the change of the NMR corresponding to a change of the effective field by $\Delta H_{\text{eff}} = 2H_C$.

We now turn to the situation where the external magnetic field is aligned perpendicular to the wire. The corresponding MR traces together with the calculated effective magnetic field are plotted in Fig. 3(b). At high field, both R and H_{eff} are linear as a function of the external field. In this region, the magnetization is aligned with the external field ($\varphi_M = 90°, \varphi_H = 90°$). This holds for $H_0 > H_A$. At $H_0 = H_A$, H_{eff} becomes, according to Eq. (2), zero. This leads to a maximum in the resistance; the NMR is at its maximum value at zero effective magnetic field. By decreasing the external field further, the interplay of the external field and internal anisotropy results in a rotation of $\vec{M}$ towards the magnetic easy axis. This rotation is reflected by a continuous increase of H_{eff}, accompanied by a corresponding decrease in resistance. For different nanowires we observe values for $\mu_0 H_A$ in the range of 1.3 to 2.2 T.

Fixing the magnetic field direction and rotating the sample in plane allows to study the angular dependence of the magnetoresistance. This is shown for sample B in Fig. 4(a) (green dots) in which the resistance R is shown as a function of φ_M for $\mu_0 H_0 = 3$ T. For high magnetic fields ($H_0 > H_A$) Eq. (2) can be simplified to $H_{\text{eff}} \approx H_0 + H_A \cos(2\varphi_M)$ since the magnetization is then nearly aligned with the external magnetic field and $\cos(\varphi_M - \varphi_H) \approx 1$. In Fig. 4(a) $R(\varphi_M)$ can be well fitted by $\cos(2\varphi_M)$, showing that the effective magnetic field dominates the magnetotransport behavior. The remaining small differences between the data and the $\cos(2\varphi_M)$ fit are expected to reflect deviations from the assumed linear relationship between the measured resistance and H_{eff}.

As the direction of the magnetic easy axis and the direction of the current coincide, the AMR effect shows the same angular dependence as one would expect from NMR. Thus the angular dependence does not allow one to distinguish between the AMR and the spin-disorder scattering induced effects proposed here. However, the typical amplitude of

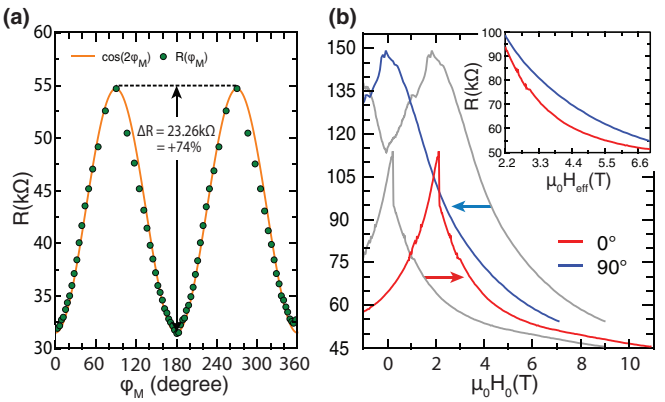

FIG. 4. (Color) (a) Dependence of the magnetoresistance on φ_m at $T = 4$ K and $\mu_0 H_0 = 3$ T (green dots): The resistance values are obtained from a measurement of $R(\varphi_H)$, while the corresponding values of φ_M are calculated by minimizing Eq. (1) for a given value of H_0 and φ_H. $R(\varphi_M)$ can be well fitted by $\cos(2\varphi_M)$ (orange curve) which describes approximately the angular dependence of the effective magnetic field. (b) Illustration of the transformation from the $\mu_0 H_0$ to the $\mu_0 H_{\text{eff}}$ scale, by shifting $R(90°)$ and $R(0°)$ by $\pm\mu_0 H_A$. The resulting high field magnetoresistance at 4 K as a function of the effective magnetic field is shown in the inset. This makes the two curves directly comparable for values of the effective field of $\mu_0 H_{\text{eff}} > 2.2$ T.

the AMR effect is below 10%,[22] thus the observed MR effect of 74% can only partly be caused by AMR. The calculations of H_{eff} for the low and high resistance states give $\mu_0 H_{\text{eff}}(\varphi_M = 0) = \mu_0(H_0 + H_A) = 4.8$ T and $\mu_0 H_{\text{eff}}(\varphi_M = 90) = \mu_0(H_0 - H_A) = 1.2$ T, which represents a difference in H_{eff} of 75%, and corresponds well to the amplitude of the MR. This, together with the well-working $\cos(2\varphi_M)$ fit of the data shown in Fig. 4(a), support the model we have put forward.

For a direct comparison of the magnetoresistance for parallel and perpendicular field configurations, the traces need to be displayed as a function of H_{eff}. For $\varphi_H = 0^\circ$ and $H_0 > H_C$, $H_{\text{eff}} = H_0 + H_A$ holds while for $\varphi_H = 90^\circ$ and $H_0 > H_A$ the effective magnetic field is $H_{\text{eff}} = H_0 - H_A$. Thus for a 0° sweep the charge carriers experience at the same H_0 an effective magnetic field which is by $2H_A$ larger than that for a 90° sweep. By simply shifting both curves by $\mu_0 H_A$ along the H_0 axis to the right and to the left, respectively [Fig. 4(b) colored lines], the two data sets nearly lie on top of each other for $H_{\text{eff}} > H_A + H_C$ [Fig. 4(b) inset], thus underpinning the dominating role of the effective magnetic field for the observed magnetoresistance. The remaining difference of 3% to 10% is most likely caused by the AMR effect.

Finally, we note that the small upward cusp, observed if the magnetic field is aligned parallel to the lithographically etched wire [red trace in Fig. 2(b)] can be ascribed to the same effect discussed above. Similar features were also observed by others.[17,24] As the magnetic field is aligned along the wire's easy axis, the AMR effect cannot contribute. The fact that the jump occurs at very low magnetic field and is small ($\sim$10 Ω), hardly resolved on the scale of Fig. 2(b), reflects the weak NMR effect and the low anisotropy field in this particular material.

In conclusion we have performed magnetotransport measurements on individually contacted GaAs/(Ga,Mn)As core-shell nanowires. By virtue of the large anisotropy field and the pronounced negative magnetoresistance effect the nanowires exhibit, we could show that the NMR of the nanowires is determined by the effective magnetic field rather than the external magnetic field. In this respect it is similar to the magnon magnetoresistance effect observed in permalloy nanowires.[25] This indicates that spin disorder scattering is the dominating mechanism responsible for the large NMR effect in GaAs/(Ga,Mn)As core-shell nanowires.

ACKNOWLEDGMENTS

We thank T. Dietl, T. Wojtowicz, G. Bayreuther, and C. Back for discussions, and M. Kiessling for performing the SQUID measurements. Support from the Deutsche Forschungsgemeinschaft (DFG) via SFB 689 is gratefully acknowledged. We thank A. Petroutchik and L. T. Baczewski for the preparation of the Au-covered substrates for NW growth.

[1] H. Ohno, A. Shen, F. Matsukura, A. Oiwa, A. Endo, S. Katsumoto, and Y. Iye, Appl. Phys. Lett. **69**, 363 (1996).
[2] T. Jungwirth, J. Mašek, J. Kučera, and A. H. MacDonald, Rev. Mod. Phys. **78**, 809 (2006).
[3] F. Matsukura, H. Ohno, A. Shen, and Y. Sugawara, Phys. Rev. B **57**, 2037 (1998).
[4] F. Matsukura, M. Sawicki, T. Dietl, D. Chiba, and H. Ohno, Phys. E (Amsterdam, Neth.) **21**, 1032 (2004).
[5] T. Omiya, F. Matsukura, T. Dietl, Y. Ohno, T. Sakon, M. Motokawa, and H. Ohno, Phys. E (Amsterdam, Neth.) **7**, 976 (2000).
[6] L. Li, S. D. Yao, S. Zhou, D. Bürger, O. Roshchupkina, S. Akhmadaliev, A. W. Rushforth, R. P. Campion, J. Fassbender, M. Helm, B. L. Gallagher, C. Timm, and H. Schmidt, J. Phys. D: Appl. Phys. **44**, 099501 (2011).
[7] J. C. Harmand, G. Patriarche, N. Péré-Laperne, M.-N. Mérat-Combes, L. Travers, and F. Glas, Appl. Phys. Lett. **87**, 203101 (2005).
[8] W. Paschoal, S. Kumar, C. Borschel, P. Wu, C. M. Canali, C. Ronning, L. Samuelson, and H. Pettersson, Nano Lett. **12**, 4838 (2012).
[9] A. Rudolph, M. Soda, M. Kiessling, T. Wojtowicz, D. Schuh, W. Wegscheider, J. Zweck, C. Back, and E. Reiger, Nano Lett. **9**, 3860 (2009).
[10] J. Liang, J. Wang, A. Paul, B. J. Cooley, D. W. Rench, N. S. Dellas, S. E. Mohney, R. Engel-Herbert, and N. Samarth, Appl. Phys. Lett. **100**, 182402 (2012).
[11] M. Hilse, Y. Takagaki, J. Herfort, M. Ramsteiner, C. Herrmann, S. Breuer, L. Geelhaar, and H. Riechert, Appl. Phys. Lett. **95**, 133126 (2009).
[12] D. V. Baxter, D. Ruzmetov, J. Scherschligt, Y. Sasaki, X. Liu, J. K. Furdyna, and C. H. Mielke, Phys. Rev. B **65**, 212407 (2002).
[13] F. Glas, G. Patriarche, L. Largeau, and A. Lemaître, Phys. Rev. Lett. **93**, 086107 (2004).
[14] F. Glas, J. C. Harmand, and G. Patriarche, Phys. Rev. Lett. **99**, 146101 (2007).
[15] The large error is a consequence of the uncertainty of the magnetically active sample volume for the nanowire array ensemble. The volume was estimated using the nanowire density determined by evaluating SEM images.
[16] J. Wenisch, C. Gould, L. Ebel, J. Storz, K. Pappert, M. J. Schmidt, C. Kumpf, G. Schmidt, K. Brunner, and L. W. Molenkamp, Phys. Rev. Lett. **99**, 077201 (2007).
[17] S. Hümpfner, K. Pappert, J. Wenisch, K. Brunner, C. Gould, G. Schmidt, L. Molenkamp, M. Sawicki, and T. Dietl, Appl. Phys. Lett. **90**, 102102 (2007).
[18] F. Hoffmann, G. Woltersdorf, W. Wegscheider, A. Einwanger, D. Weiss, and C. H. Back, Phys. Rev. B **80**, 054417 (2009).
[19] M. Schlapps, T. Lermer, S. Geissler, D. Neumaier, J. Sadowski, D. Schuh, W. Wegscheider, and D. Weiss, Phys. Rev. B **80**, 125330 (2009).
[20] J. Wunderlich, T. Jungwirth, B. Kaestner, A. C. Irvine, A. B. Shick, N. Stone, K. Y. Wang, U. Rana, A. D. Giddings, C. T. Foxon, R. P. Campion, D. A. Williams, and B. L. Gallagher, Phys. Rev. Lett. **97**, 077201 (2006).
[21] A wire array consisting of 25 nanostripes, each with a width of 42 nm and a length of 7.5 μm was used to suppress universal conductance variations, see Ref. 26.
[22] A. W. Rushforth, K. Výborný, C. S. King, K. W. Edmonds, R. P. Campion, C. T. Foxon, J. Wunderlich, A. C. Irvine, P. Vašek,

V. Novák, K. Olejník, J. Sinova, T. Jungwirth, and B. L. Gallagher, Phys. Rev. Lett. **99**, 147207 (2007).
[23]L. Landau, Phys. Z. Sowjetunion **8**, 14 (1935).
[24]S. T. B. Goennenwein, S. Russo, A. F. Morpurgo, T. M. Klapwijk, W. Van Roy, and J. De Boeck, Phys. Rev. B **71**, 193306 (2005).
[25]V. D. Nguyen, C. Naylor, L. Vila, A. Marty, P. Laczkowski, C. Beigné, L. Notin, Z. Ishaque, and J. P. Attané, Appl. Phys. Lett. **99**, 262504 (2011).
[26]D. Neumaier, K. Wagner, U. Wurstbauer, M. Reinwald, W. Wegscheider, and D. Weiss, New J. Phys. **10**, 055016 (2008).